

Kinetics of Random Sequential Adsorption of Interacting Particles on Partially Covered Surfaces

by

Paweł WEROŃSKI

Presented by Jerzy HABER on October 14, 2003

Summary. The random sequential adsorption (RSA) approach was used to analyse adsorption kinetics of charged spheres at charged surfaces precovered with smaller sized, likely charged particles. The algorithm of M. R. Oberholzer *et al.* [20] was exploited to simulate adsorption allowing electrostatic interaction in three dimensions, that is, particle-particle and particle-surface interactions during the approach of a particle to the substrate. The calculation of interaction energies in the model was achieved with the aid of a many-body superposition approximation. The effective hard particle approximation was used for determination of corresponding simpler systems of particles, namely: the system of hard spheres, the system of particles with perfect sink model of particle-interface interaction, and the system of hard discs at equilibrium. Numerical simulations were performed to determine adsorption kinetics of larger particles for various surface concentration of smaller particles. It was found that in the limit of low surface coverage the numerical results were in a reasonable agreement with the formula stemming from the scaled particle theory with the modifications for the sphere-sphere geometry and electrostatic interaction. The results indicate that large particle-substrate attractive interaction significantly reduces the kinetic barrier to the large, charged particle adsorption at a surface precovered with small, likely charged particles.

Localised, irreversible adsorption phenomena can be modeled using a variety of approaches. Among them, the random sequential adsorption (RSA) approach seems to be the most common one due to its simplicity and efficiency. The classical RSA model considers a sequence of trials of a particle adsorption at a homogeneous interface [1–3]. Once an empty surface element is found the particle is permanently fixed with no consecutive motion allowed. Otherwise, the virtual particle is rejected and a next addition at-

Key words: adsorption of colloids, colloid particle adsorption, irreversible adsorption, particle deposition, heterogeneous surface adsorption, colloidal electrostatic interactions, superposition approximation, Monte-Carlo simulation.

tempt is undertaken. Since the 80s a number of extended RSA models were developed including effects of particle shape [4–8], Brownian motion [9–12], external force [13–16], particle-particle [17–19] and particle-interface [20] electrostatic interaction, colloid particle polydispersity [21–23], and surface heterogeneity [24–27]. The results based on RSA simulations allow prediction of particle monolayer structure and jamming coverage of particles. One may use the model to predict particle adsorption kinetics as well, although depending on the particle transport mechanism, an appropriate analysis of real adsorption problems can require including a correction for bulk transport or the hydrodynamic scattering effect [28]. Thus, the RSA modeling can be a powerful tool in the study of irreversible adsorption of macromolecules, proteins, and colloid particles.

However, in spite of these new developments, the current state of art is still far from complete. Usually, an adequate description of a real experiment requires that more than one effect at once should be considered. This is especially the case when one deals with adsorption at heterogeneous surfaces. Existing literature on effects of surface heterogeneity in colloid adsorption is limited to the simplest system of spherical, monodisperse, hard (non-interacting) particles. These models seem inadequate for a broad range of practical situations because real particles in electrolyte usually bear electrostatic charge, so particle-particle or particle-interface electrostatic interaction should be taken into consideration.

This paper focuses on the effect of electrostatic interaction on colloid adsorption kinetics at surfaces precovered with smaller sized, likely charged particles. Both particle-particle (repulsive) and particle-interface (attractive) interactions are included in the model. The electrostatic interaction approach presented in Ref. [20] is generalized to a bimodal system of spherical particles. On the other hand, the results presented in the paper are generalization of the results published in Ref. [25], obtained for non-interacting particles. Particle adsorption kinetics presented in the paper was determined from numerical simulations performed according to the Monte-Carlo scheme. The effective hard particles system concept was exploited as a tool for determination of corresponding simpler systems, namely: the system of hard spheres, the system of particles with perfect sink model of particle-interface interaction, and the system of hard discs at equilibrium. The results were obtained for one particular system of particles and the adsorption kinetics were simulated just for a few selected values of the small particles coverage. Nevertheless, the results demonstrate general trends and allow verification of the simplified models.

The Theoretical Model

3D Electrostatic Interaction Model. An exact determination of the interaction energy between particles near the adsorption surface in the general case seems prohibitive due to the inherent many-body problem. However, as demonstrated in Ref. [20], in the case of short-ranged interactions and not very low surface potentials the van der Waals attraction is negligible and the superposition approximation of the electrostatic interaction offers satisfactory accuracy of the total particle potential at the precovered collector surface. We adopt the 3D RSA model presented in Ref. [20] and assume that neither electrostatic interaction nor Brownian motion causes a shift in the lateral position of the adsorbing particle as it moves toward the collector surface. Although the authors of Ref. [20] claim that the 3D RSA model is more realistic, one should remember that physics of this approach is still greatly simplified. During this motion the total particle potential can be calculated according to the formula

$$(1) \quad E_i(h) = \sum_{m=1}^n E_{ij}(h_m) + E_{ip}(h), \quad i, j = l, s$$

where h is the particle-interface gap width, n is the number of the small and large particles attached to the collector surface in the vicinity of the adsorbing particle, h_m is the minimum surface-to-surface distance between the moving particle and the deposited particle m , E_{ij} is the electrostatic (repulsive) interaction energy between them, and E_{ip} is the electrostatic (attractive) interaction energy between the particle and the collector surface. In what follows the subscripts s and l correspond to the small and large particle, respectively. We assume constant potential on all surfaces and model all electrostatic interactions in the system using the linear superposition approximation (LSA) of Bell *et al.* [29]. For two spherical particles of radii a_i and a_j , separated by gap width h_m , the repulsive energy is

$$(2) \quad E_{ij}(h_m) = \varepsilon \frac{kT}{e^2} Y_i Y_j \frac{a_i a_j}{a_i + a_j + h_m} \exp(-\kappa h_m)$$

where ε is the dielectric constant of the medium, k is the Boltzmann constant, T is the absolute temperature, e is the electron charge, κ^{-1} is the Debye length, and Y_i and Y_j are the effective surface potentials of the particles given by the equation [30]

$$(3) \quad Y_m = \frac{8 \operatorname{tg} h(\bar{\psi}_m/4)}{1 + \sqrt{1 - \frac{2\kappa a_m + 1}{(\kappa a_m + 1)^2} \operatorname{tg} h^2(\bar{\psi}_m/4)}}, \quad m = i, j$$

where $\bar{\psi}_m = \psi_m \frac{e}{kT}$ is dimensionless surface potential of the particle m , and ψ_m is its surface potential. The attractive electrostatic energy between

the traveling spherical particle and the adsorption surface is given by the limiting forms of Eqs. (2) and (3) when one of the particles radii tends to infinity.

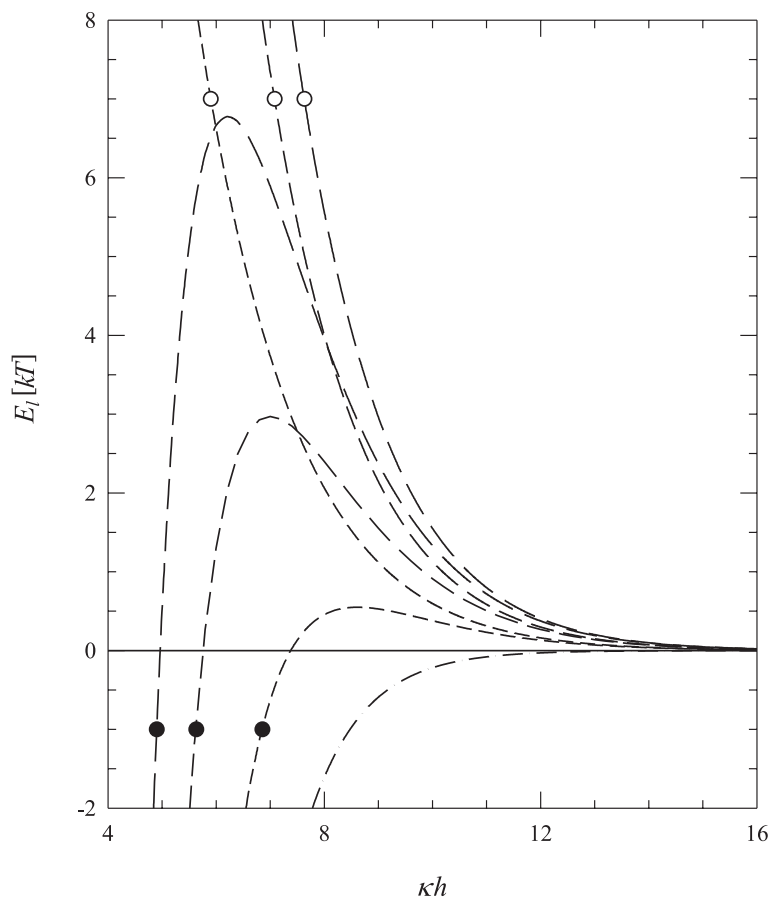


Fig. 1. Electrostatic interaction energy profiles calculated for the large particle approaching the surface next to the small particle in 3D RSA. The plots represent results based on Eq. (1). The solid line with empty square depicts large particle-interface attraction. The empty and filled circle indicates particle-particle repulsion and the total energy profiles, respectively. The solid, dashed, and dotted lines correspond to $r_2 = r_0 + 2/\kappa$, $r_2 = r_0 + 1.2/\kappa$, and $r_2 = r_0 + 0.8/\kappa$, respectively, where $r_0 = 2\sqrt{a_s a_l}$

In general, a total interaction energy profile $E_i(h)$ is produced by combination of the repulsion exerted by the attached particles with the attraction exerted by the surface. As a consequence, the profile has a maximum $E_b(x_i, y_i, x_j, y_j)$, which represents a kinetic barrier to adsorption of the virtual particle and its height depends on configuration of deposited small and large particles. Figure 1 presents the total interaction energy profiles cor-

responding to the simplest system of the large particle moving toward the surface next to the small, adsorbed particle. The profiles correspond to the system studied using RSA computer simulations as described later on, and to three different values of the particles center-to-center distance projection length $r_2 = \sqrt{(x_l - x_s)^2 + (y_l - y_s)^2}$, where x_l , x_s , y_l and y_s are the particles coordinates. Based on the plots one can conclude that the energy barrier occurs at some height above the adsorption surface and the barrier height increases when the projection length r_2 decreases. This trend can be more clearly observed in Fig. 2 presenting kinetic barrier to adsorption plotted as a function of the projection length $E_b(r_2)$.

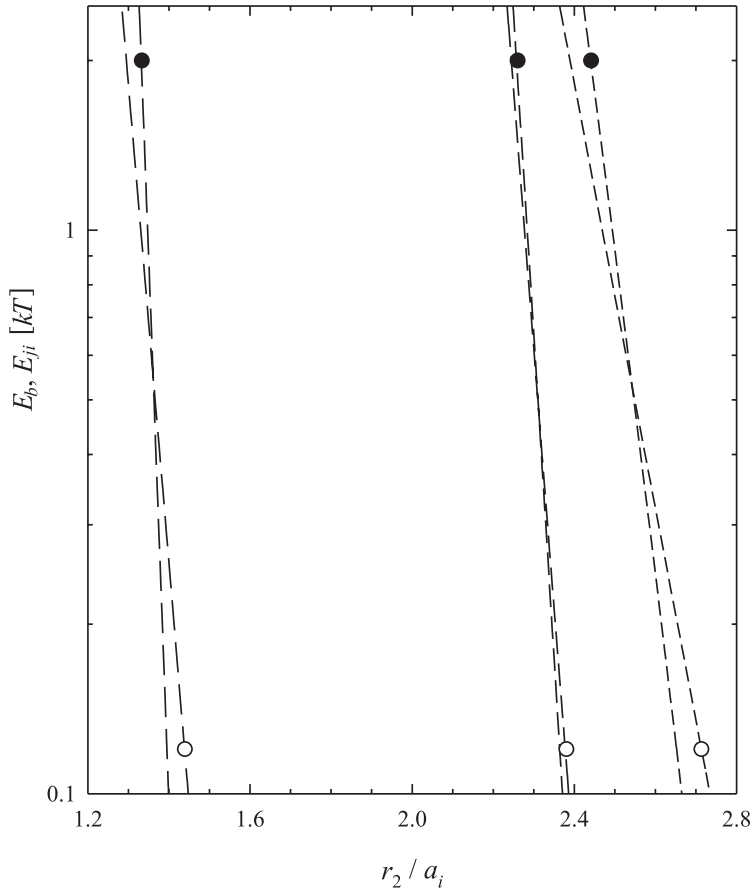


Fig. 2. Kinetic barrier to particle adsorption in 2D RSA and 3D RSA models for three different systems of particles. The filled and empty circle depicts 3D and 2D model predicted results, respectively. The dotted and solid lines correspond to the system of two small ($i = s$, $j = s$) and two large ($i = l$, $j = l$) particles at the interface, respectively. The dashed lines present energy barrier for the large particle approaching to the substrate next to the adsorbed small particle ($i = l$, $j = s$)

Simplified Models of Interaction. One can simplify modeling of the electrostatic interaction by exploiting the effective hard particles system concept. Following the idea of Barker and Henderson [31] we introduce the effective hard particles center-to-center distance projection length given by

$$(4) \quad d_{ij} = \int_0^{\infty} \{1 - \exp[-E_b(r_2)]\} dr_2$$

where in general $r_2 = \sqrt{(x_i - x_j)^2 + (y_i - y_j)^2}$ and $i, j = s, l$. Thus, the parameters d_{ij} can be determined by the numerical integration according to Eq. (4) provided that function $E_b(r_2)$ is known. We assume that energy barrier tends to infinity when the two particles overlap ($r_2 < 2\sqrt{a_i a_j}$), and for larger values of the argument the function can be calculated numerically as described in Ref. [20]. In our study we used Ridders method [32] and looked for the E_b value exploiting the condition $\frac{dE_i}{dh} = 0$ (vanishing of the first derivative).

Another concept of the effective hard particles system, which we tested in our simulations, was introduced by Piech and Walz [33]. Adopting their idea, the effective hard particles center-to-center distance projection length can be defined as the projection length corresponding to the energy barrier equal to $0.5 kT$:

$$(5) \quad d_{ij} = r_2^*, \quad E_b(r_2^*) = 0.5$$

In our calculations of the parameters d_{ij} we solved the system of two non-linear equations: $\frac{dE_i}{dh} = 0$ and $E_i(h) = 0.5$ applying the subroutine DNSQ of the SLATEC library [34], which uses a modification of the Powell hybrid method.

Knowing d_{ij} one can replace the time-consuming computations of the energy barrier and estimation of the particle adsorption probability, as described later on, with a simple comparison of the projection length r_2 and parameters d_{ij} . The case $r_2 < d_{ij}$ corresponds to the infinite energy of the particle-particle interaction. The particles do not interact if $r_2 > d_{ij}$. Note that the particle-interface interaction is included into the parameters d_{ij} and it is not considered explicitly in the model. In what follows we call this model of interaction the effective hard sphere (EHS) model.

Another simplified model of the electrostatic interaction existing in literature is the approach introduced by Adamczyk *et al.* in Ref. [17] and exploited in Refs. [18–20, 23–24, 28]. The model called 2D RSA takes into account only lateral, Yukawa-type interactions between particles on the surface and assumes perfect sink model of the interaction between the particles and the adsorption surface. Although the electrostatic particle-surface interaction is not directly included, the Yukawa form of the interparticle potential used in the model contains the fitting parameter E_{ij}^0 allowing for some kind

of correction for the surface interaction:

$$(6) \quad E_{ij}(h_k, E_{ij}^0) = E_{ij}^0 \frac{a_i}{a_i + a_j + h_k} \exp(-\kappa h_k)$$

where $i, j = s, l$. Note that the total lateral interaction, calculated using superposition approximation, represents the kinetic barrier to the particle adsorption in 2D model.

Exploiting the idea of the effective hard particle one can avoid introducing the fitting parameter into the model. This can be achieved by comparing of the 2D model with a 3D model, which includes particle-surface interaction. More specific, we can find the corresponding 2D and 3D systems comparing the effective hard particles center-to-center distance projection lengths. In our study we used 3D RSA model described above. Under assumption of Barker-Henderson approximation one can calculate the E_{ij}^0 parameters using the equation

$$(7) \quad \int_0^{\infty} \{\exp[-E_b(r_2)] - \exp[-E_{ij}(h_k, E_{ij}^0)]\} dr_2 = 0$$

derived by exploiting Eq. (4), where $h_k = \sqrt{r_2^2 + (a_i - a_j)^2} - a_i - a_j$. A variety of numerical methods can be implemented to search for a root E_{ij}^0 of nonlinear Eq. (7).

The comparison of the energy profiles $E_b(r_2)$ and the profiles $E_{ij}(r_2)$ obtained for the corresponding 2D systems using Barker-Henderson approximation is depicted in Fig. 2. The profiles were calculated for our particular system studied in simulations. As one can see, the 3D profiles change more rapidly. The corresponding 2D and 3D profiles of energy intersect at an energy value of $0.5 kT$ that suggests a good agreement with the Piech-Walz approach of the effective hard particle. According to the model the E_{ij}^0 parameters were calculated using the equation

$$(8) \quad E_{ij}^0 = \frac{\sqrt{r_2^{*2} + (a_i - a_j)^2}}{2a_i} \exp \left\{ \kappa \left[\sqrt{r_2^{*2} + (a_i - a_j)^2} - a_i - a_j \right] \right\}$$

where r_2^* is a root of equation $E_b(r_2^*) = 0.5$ found numerically as described above.

The values E_{ij}^0 based on Eqs. (7)–(8) and d_{ij} calculated using Eq. (4) for our particular system are summarized in Table 1. As one can see, both models give similar results. Therefore, one can expect similar adsorption kinetics too. Note that large-small particle interaction is greatly reduced as suggests the E_{ls}^0 parameter, which is over twenty times smaller than E_{ss}^0 parameter corresponding to the system of two small particles. This effect, resulting from the particle-surface interaction, is in agreement with the experimental results presented in Ref. [24]. Although the authors of the

T A B L E 1

Parameters d_{ij} and E_{ij}^0 estimated for the system studied in RSA simulations

i	j	d_{ij} [nm]	E_{ij}^0 [kT] ^(*)	E_{ij}^0 [kT] ^(**)
s	s	633.93	120.80	115.69
l	s	850.31	5.05	4.34
l	l	1440.43	716.03	710.74

(*) Barker–Henderson approximation

(**) Piech–Walz approximation

note suggested that the reduced electrostatic interaction could result from the colloid particles charge migration at the mica surface, in view of the present results one can explain the observed effect based on reduction of the different sized particles interaction at the charged adsorption surface.

If one neglects the effect of the interface then E_{ij}^0 values can be deduced directly from Eq. (2). In our particular system the limiting values of E_{ss}^0 and E_{ll}^0 parameters are equal to 590 and 1413 kT , respectively. It is interesting to note that the limiting values of the parameters are two to five times larger than the values calculated for the corresponding systems allowing the particle-interface interaction, which is in good agreement with the results reported in Ref. [17].

Simulation Methods

3D RSA Simulation Method. The simulation algorithm was similar to that used for bimodal sphere adsorption described in Ref. [25]. The simulations were carried out over a square simulation plane with the usual periodic boundary conditions at its perimeter. The simulation plane was divided into two subsidiary grids of square areas (cells) of the size $\sqrt{2}a_s$ and $\sqrt{2}a_l$. This enhanced the scanning efficiency of the adsorbing particle environment performed at each simulation step.

The entire simulation procedure consisted of two main stages. First, the simulation plane was covered with smaller sized particles to a prescribed dimensionless surface coverage $\theta_s = \pi a_s^2 N_s$, where N_s is the surface number density of the smaller particles. Then the larger spheres were adsorbed at the precovered surface. At both stages the overlapping test was carried out by considering the three-dimensional distances between the sphere centers. If there was no overlapping the kinetic barrier to adsorption E_b was calculated using 3D interaction model as described above. The tested vicinity of the virtual particle was limited to the circle of radius r_c , chosen such that $E_{ij}(r_c) = 0.01 kT$. The virtual particle was adsorbed with the probability p

given by the Boltzmann relationship. This was done through generating an additional random number p_r with uniform distribution within the interval $(0; 1)$. Particle adsorption took place when p was larger than p_r .

In order to simulate the kinetic runs the dimensionless adsorption time τ was set to zero at the beginning of the second stage. In our calculations τ was defined as

$$(9) \quad \tau = \frac{n_{att}}{n_{ch}}$$

where n_{att} and n_{ch} are the overall and the characteristic number of the large particle adsorption trials, respectively. The characteristic attempt number is usually defined as $n_{ch} = S/\pi a_l^2$, where S is the adsorption plane surface area. The maximum dimensionless time attained in our simulations was 10^4 , which required n_{att} of order 10^9 .

Simplified Simulation Methods. Since 3D RSA simulations including numerical calculation of the kinetic barrier to particle adsorption E_b at each simulation loop are time consuming (especially at higher surface concentrations) the simplified adsorption models seem attractive from a practical viewpoint. The RSA algorithm using EHS approximation is very efficient because no electrostatic interaction is calculated during the simulation loop. More specific, the regular overlapping test, the subroutine evaluating the energy barrier and adsorption probability is replaced by the modified overlapping test comparing the variable r_2 with the corresponding parameter d_{ij} rather than with the geometrical overlapping distance equal to $2\sqrt{a_l a_s}$. The rest of the simulation procedure is similar to the 3D RSA algorithm.

Unlike the EHS approach, the simplified 2D interaction model employed in RSA simulations requires to calculate the interaction energy for all particles in the vicinity of the test particle during each loop of the simulation. Technically, the algorithm differs from the 3D RSA model in that it avoids numerical looking for the energy barrier. Thus, the computational gain is not very large. However, the 2D model has been exploited in computer simulations for a few years and comparison with the 3D model seems interesting.

Analytical Approximation

Due to a lack of appropriate expressions for the adsorption kinetics in the case of RSA of large particles at precovered surfaces, we test our results in terms of the equilibrium adsorption approaches. In view of the results obtained for bimodal systems of hard particles [24–25, 35] this seems reasonable at an early stage of the adsorption process at low surface coverage.

We generalize the derivation published in Ref. [25] to a system of interacting particles exploiting the effective hard particle concept. According

to the scaled particle theory (SPT) formulated in Ref. [36] and then extended to multicomponent mixtures in Refs. [37–38], the equilibrium large disk available surface function (ASF) for bimodal suspension of disks is given by the expression

$$(10) \quad \phi_{ld} = -\ln\left(\frac{\mu_{ld}^R}{kT}\right) \\ = (1 - \theta_d) \exp\left[-\frac{3\theta_{ld} + \gamma(\gamma + 2)\theta_{sd}}{1 - \theta_d} - \left(\frac{\theta_{ld} + \gamma\theta_{sd}}{1 - \theta_d}\right)^2\right]$$

where μ_{ld}^R is the residual potential of the larger particles, $\theta_{id} = \pi a_{id}^2 N_{id}$ is the disk surface coverage, $i = l, s$, a_{id} and N_{id} are the disk radius and surface number density, respectively, $\theta_d = \theta_{ld} + \theta_{sd}$, and $\gamma = a_{ld}/a_{sd}$ is the disk size ratio. It should be noted that Eq. (10) describes a two-dimensional system only.

However, a useful approximation of the hard sphere adsorption can be formulated by redefining the geometrical parameter γ . Expanding Eq. (10) in the power series of θ_{id} (up to the order of two) one obtains the expression

$$(11) \quad \phi_{ld} \cong 1 - 4\theta_{ld} - (\gamma + 1)^2\theta_{sd}$$

valid for low surface coverage. In the case of bimodal spheres system it can be deduced from geometrical consideration that at low coverage the large particle ASF is equal to

$$(12) \quad \phi_l \cong 1 - 4\theta_l - 4\lambda\theta_s$$

where λ is the large-to-small sphere size ratio $\lambda = a_l/a_s$. Thus, Eqs. (11) and (12) can be matched when

$$(13) \quad \gamma = 2\sqrt{\lambda} - 1,$$

$\theta_{ld} = \theta_l$, and $\theta_{sd} = \theta_s$. We can conclude that a bimodal disks system corresponds (in a sense of ASF) to a bimodal spheres system if Eq. (13) is fulfilled. This means that ASF of the large sphere can be approximated by Eq. (10), where the corresponding disk size ratio is defined by Eq. (13).

Now, let us consider a bimodal sphere system composed of hard small particles and soft (interacting) large particles. It is not difficult to find from elementary geometry that in the limit of low coverage the ASF for the large sphere is given by

$$(14) \quad \phi_l \cong 1 - 4\left(\frac{d_{ll}}{2a_l}\right)^2\theta_l - 4\lambda\theta_s$$

Thus, Eq. (10) describes ASF of the large interacting spherical particle in the low coverage limit if one substitutes Eq. (13), replaces θ_{sd} with θ_s and θ_{ld} with $(d_{ll}/2a_l)^2\theta_l$.

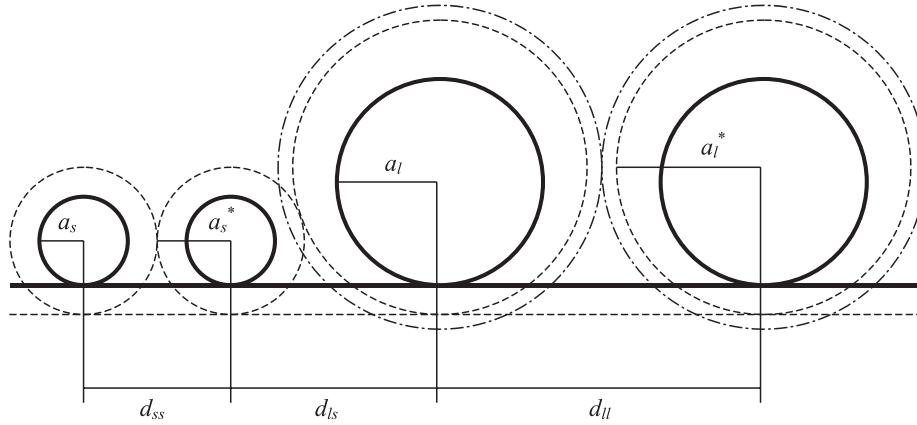


Fig. 3. Effective hard small and soft large particles. The thick line depicts the real geometrical shapes of the particles and interface. The dashed lines denotes shapes of the effective particles and adsorption surface. The dash-dot line shows the effective interaction range of the large particles

Knowing d_{ij} parameters of a bimodal soft spheres system one can find the corresponding system of the hard small and soft large particles. From the symmetry condition we have

$$(15) \quad a_s^* = \frac{1}{2}d_{ss}$$

and from the Pythagorean Theorem $d_{ls}^2 + (a_l^* - a_s^*)^2 = (a_l^* + a_s^*)^2$ we get

$$(16) \quad a_l^* = \frac{d_{ls}^2}{4a_s^*} = \frac{d_{ls}^2}{2d_{ss}}$$

(see Fig. 3), where variables with a star denote quantities corresponding to the effective particles. The effective size ratio is given as

$$(17) \quad \lambda^* = \frac{a_l^*}{a_s^*} = \left(\frac{d_{ls}}{d_{ss}}\right)^2$$

and surface coverage of the effective small and large particles equals, respectively,

$$(18) \quad \theta_s^* = \theta_s \left(\frac{a_s^*}{a_s}\right)^2 = \theta_s \left(\frac{d_{ss}}{2a_s}\right)^2$$

$$(19) \quad \theta_l^* = \theta_l \left(\frac{a_l^*}{a_l}\right)^2 = \theta_l \left(\frac{d_{ls}^2}{2a_l d_{ss}}\right)^2$$

Exploiting Eq. (14) we get the large particle ASF in the low coverage

limit

$$(20) \quad \phi_l \cong 1 - 4 \left(\frac{d_{ll}}{2a_l^*} \right)^2 \theta_l^* - 4\lambda^* \theta_s^*$$

Eqs. (11) and (20) can be matched when

$$(21) \quad \theta_{ld} = \left(\frac{d_{ll}}{2a_l^*} \right)^2 \theta_l^* = \left(\frac{d_{ll}}{2a_l} \right)^2 \theta_l$$

$$(22) \quad \theta_{sd} = \theta_s^* = \left(\frac{d_{ss}}{2a_s} \right)^2 \theta_s$$

$$(23) \quad \gamma = 2\sqrt{\lambda^*} - 1 = 2 \frac{d_{ls}}{d_{ss}} - 1$$

Finally, we conclude that the ASF for the large sphere in the bimodal interacting spherical particles system in the limit of the low coverage can be approximated by equation

$$(24) \quad \phi_l = (1 - \theta_d) \exp \left[- \frac{3\theta_{ld} + \gamma(\gamma + 2)\theta_{sd}}{1 - \theta_d} - \left(\frac{\theta_{ld} + \gamma\theta_{sd}}{1 - \theta_d} \right)^2 \right]$$

where variables θ_{ld} , θ_{sd} and γ are defined by Eqs. (21)–(23), respectively.

Knowing ϕ_l one can calculate particle adsorption kinetics from the constitutive dependence [2–7]

$$(25) \quad \phi_l = \frac{d\theta_l}{d\tau}$$

This can be formally integrated to the form

$$(26) \quad \theta_l(\tau) = \left[\int_0^{\theta_l} \frac{d\xi_l}{\phi_l(\xi_l)} \right]^{(-1)}$$

where $[f(x)]^{(-1)}$ represents the inverse function of the function $f(x)$ and ξ is a dummy integration variable. It should be mentioned that Eq. (26) adequately describes the adsorption kinetics only in a system where both bulk transport and the hydrodynamic scattering effect can be neglected. In general, the extended RSA model should be employed [28].

Results and Discussion

Computer simulations were performed using the above RSA algorithms. The large particles adsorption kinetics was determined for the following values of the system physical parameters: small particle radius and surface potential $a_s = 250$ nm and $\psi_s = 50$ mV, respectively, large particle radius and surface potential $a_l = 625$ nm and $\psi_l = 50$ mV, respectively, adsorption surface potential $\psi_p = -100$ mV, absolute temperature $T = 293$ K, $1 - 1$

electrolyte concentration $c = 10^{-4}$ M, and dielectric constant $\varepsilon = 78.54$. Corresponding dimensionless parameters κa_s , κa_l , and λ^* were equal to 8.29, 20.73 and 1.80, respectively. The simulations were conducted at small particle surface coverage $\theta_s = 0$ (reference curve for the monodisperse particle system), 0.05, 0.10, 0.15, and 0.20, which corresponds to effective small particle surface coverage $\theta_s^* = 0, 0.08, 0.16, 0.24, \text{ and } 0.32$.

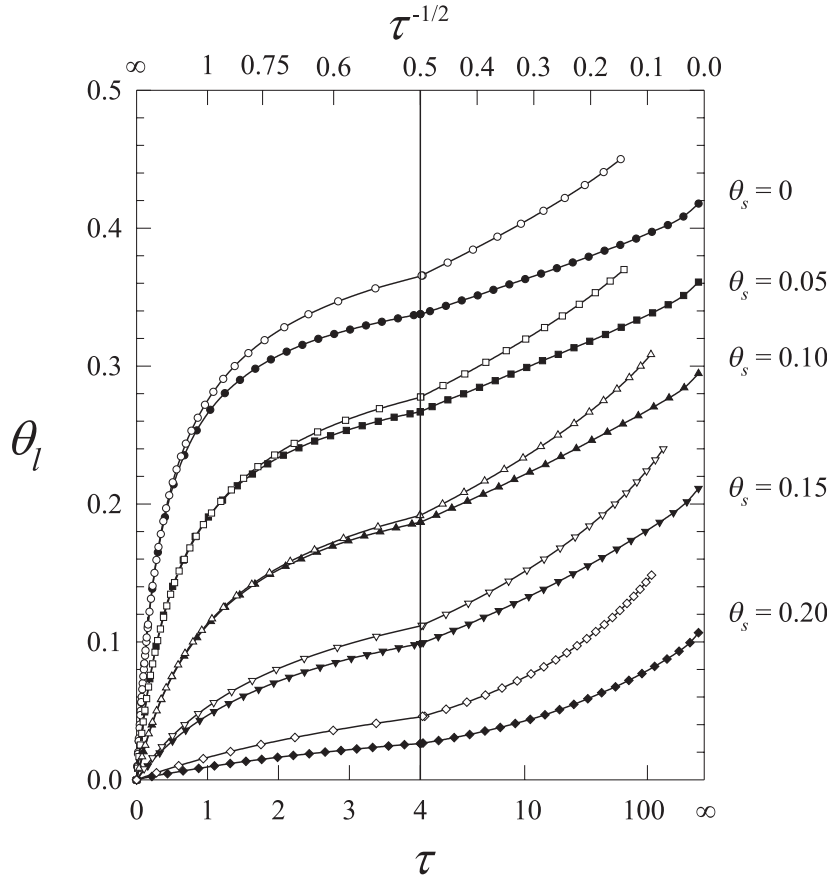


Fig. 4. Kinetics of larger particle adsorption at surfaces precovered with smaller particles expressed as θ_l vs. τ dependencies: 1 (circles) – $\theta_s = 0$; 2 (squares) – $\theta_s = 0.05$; 3 (triangles) – $\theta_s = 0.10$; 4 (reversed triangles) – $\theta_s = 0.15$; 5 (diamonds) – $\theta_s = 0.20$. The filled symbols denote 3D RSA model predicted results. The open symbols depict the analytical results for the corresponding equilibrium system of the hard disks calculated from Eq. (26)

Figure 4 depicts the dependence of θ_l on τ as obtained in simulations employing 3D RSA particle interaction model, and the analytical SPT results represented by Eq. (26) with ϕ_l given by Eq. (24). As can be noticed,

the agreement between the RSA simulations and these analytical predictions seems quantitative when $\theta_s \leq 0.10$ ($\theta_s^* \leq 0.16$) and surface coverage θ_l does not exceed 50% of its maximum value. The positive deviations of the SPT results from the RSA calculations become quite significant at higher θ_s and θ_l , which reflects a general relationship between the corresponding equilibrium and RSA processes.

In order to compress the infinite time domain into a finite one the regular independent variable τ was replaced with $\tau^{-1/2}$ at $\tau > 4$ (right-hand side of Figs. 3–6). This transformation was successfully applied previously [1–3] to present the results of RSA at uncovered surfaces when

$$(27) \quad \theta_\infty - \theta_l \propto \tau^{-1/2},$$

where θ_∞ is the jamming coverage for monodisperse spheres calculated to be 0.547. Similar long-time behavior of the surface coverage was observed for adsorption at heterogeneous surfaces [25–27].

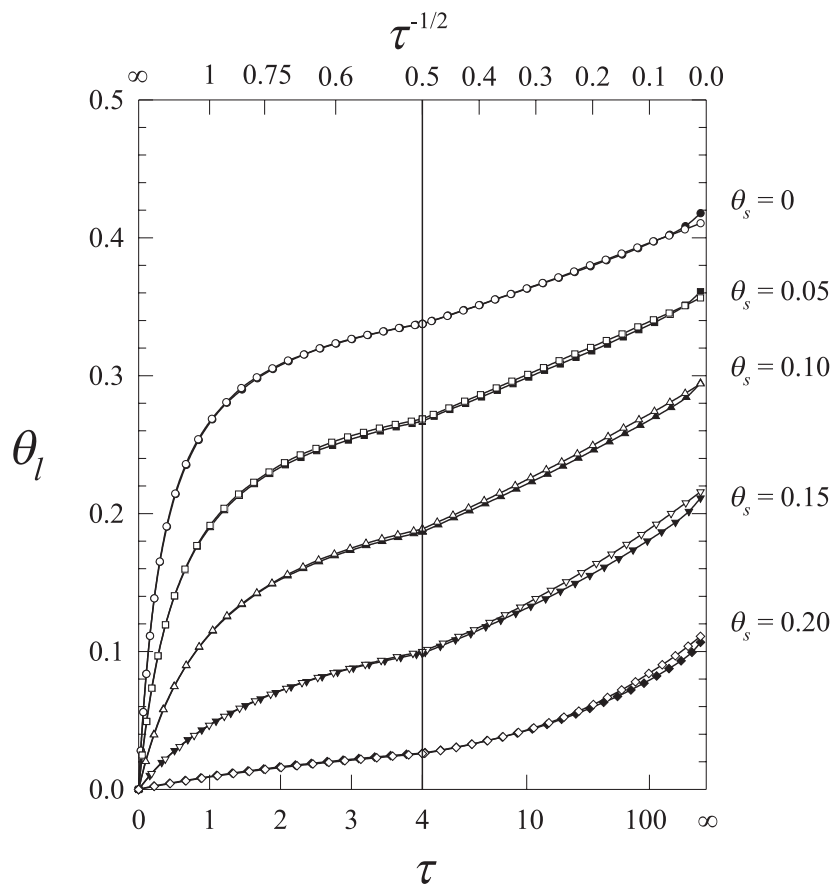


Fig. 5. Same as Fig. 4 except the open symbols depict the EHS model predicted results

In Fig. 5 a comparison of the adsorption kinetics based on 3D RSA and EHS particle interaction models is presented. It is interesting to observe that the two models give almost identical results in the whole range of surface coverage. The EHS results are slightly overestimated at the medium and high coverage regimes. This may result from the fact that the effective particle sizes used in EHS model were calculated using Eq. (4) under the assumption of the low surface coverage and uniform distribution of the particles center-to-center distance projection length r_2 . However, at high surface coverage the distribution becomes non-uniform [25] and thus Eq. (4) is less accurate at this range.

A straight-line dependence of θ_l vs. $\tau^{-1/2}$ can be observed at the long-time adsorption regime especially at $\theta \leq 0.10$. Some deviations of the EHS results from linearity are evident at very long adsorption times. The effect is similar to that of soft particle adsorption at homogeneous surface [39].

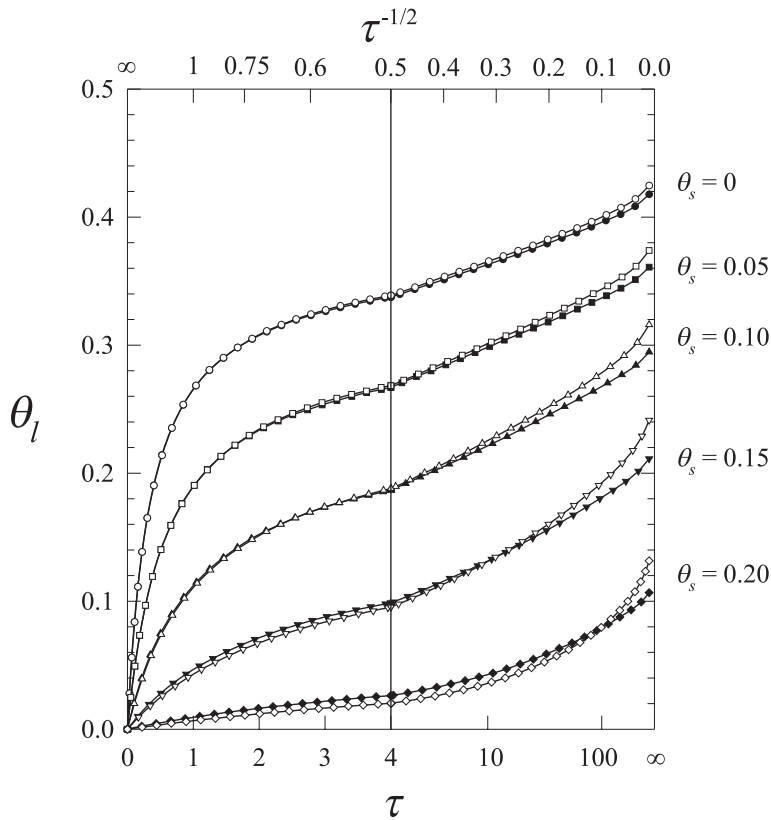


Fig. 6. Same as Fig. 4 except the open symbols denote the 2D RSA simulations using the Barker–Henderson approximation

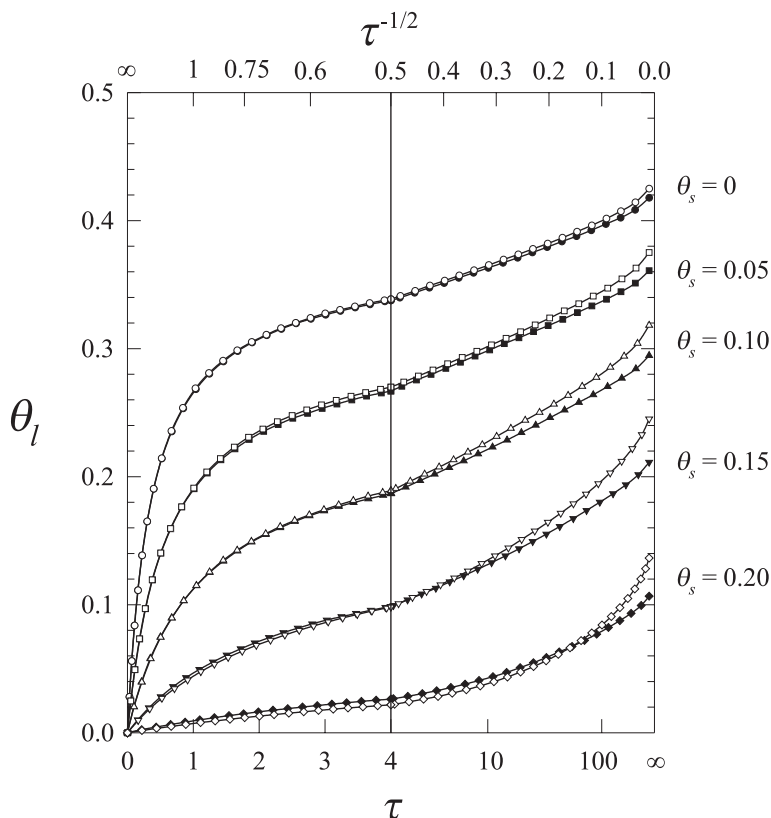


Fig. 7. Same as Fig. 4 except the open symbols denote the 2D RSA simulations using the Piech–Walz approximation

Unlike the effective hard particles, interacting particles can be adsorbed at distance r_2 smaller than d_{ij} provided that $r_2 > 2\sqrt{a_i a_j}$. Although adsorption probability in such configuration at one trial is very low, at sufficiently long adsorption time the probability tends to unity, which results in the increased adsorption kinetics at $\tau \rightarrow \infty$. It should be noted that such extremely long adsorption time seems prohibited from the experimental point of view.

Figures 6 and 7 present the results of simulations employing simplified 2D RSA models of particle interaction compared with the results obtained in 3D RSA simulations. Both the Barker–Henderson and Piech–Walz approximations give very similar results. The 2D models can be successfully used for accurate adsorption kinetics determination particularly at $\theta_s \leq 0.15$, although the results are somewhat overestimated at high surface concentration. This is consistent with the energy profiles depicted in Fig. 2. At higher surface concentration the large particle can be adsorbed just at a relatively short distance to another particle. At this range $\phi_b > \phi_{ij}$, which results in

faster adsorption kinetics in case of 2D RSA model.

Another discrepancy is visible at large θ_s when the effective hard particle approximation becomes less accurate. As one can see, the 2D model predicted results are underestimated at small to medium θ_l . The slower adsorption kinetics results from smaller initial adsorption flux. This trend cannot be explained based on the energy profiles and should be studied in terms of the layer structure and pair correlation function.

Concluding Remarks

The results presented in this paper clearly demonstrate that the numerical RSA simulations concerning interacting spherical particle adsorption at precovered surfaces can be well approximated in the limit of low densities by the extrapolated SPT with the geometrical parameter $\gamma = 2d_{ls}/d_{ss} - 1$ and surface coverage transformed to $\theta_{ld} = (d_{ll}/2a_l)^2\theta_l$ and $\theta_{sd} = (d_{ss}/2a_s)^2\theta_s$. It was also shown that the effective hard particles center-to-center distance projection lengths d_{ij} can be calculated from the effective hard particle approximation. By adopting the effective hard particle concept the simplified models of particle-particle and particle-surface interaction can be used in simulations rather than 3D RSA approach. It was found that the EHS model is the very effective and accurate one. The numerical simulations performed according to the MC-RSA algorithms confirmed validity of the simplified 2D RSA model with the corresponding values of the ϕ_{ij}^0 parameters determined from the effective hard particle approximation. The values of the parameters ϕ_{ij}^0 calculated numerically clearly suggest that the kinetic barrier to adsorption of the large particle next to the small particle is greatly reduced due to large particle-surface attraction. This prediction confirms earlier experimental results.

Acknowledgements. The author would like to thank Professor Z. Adamczyk for reading the manuscript and offering his valuable suggestions. This work was supported by the EC Grant GRD 1-2000-26823.

INSTITUTE OF CATALYSIS AND SURFACE CHEMISTRY, POLISH ACADEMY OF SCIENCES, UL.
NIEZAPOMINAJEK 8, 30-239 KRAKÓW, POLAND
(INSTYTUT KATALIZY I FIZYKOCHEMII POWIERZCHNI PAN)
e-mail: ncwerons@cyf-ir.edu.pl

REFERENCES

- [1] E. L. Hinrichsen, J. Feder, T. Jøssang, J. Stat. Phys., **44** (1986) 793.
- [2] P. Schaaf, J. Talbot, J. Chem. Phys., **91** (1989) 4401.
- [3] J. Talbot, G. Tarjus, P. Schaaf, Phys. Rev. A, **40** (1989) 4808.
- [4] P. Viot, G. Tarjus, Europhys. Lett. **13** (1990) 295.

- [5] G. Tarjus, P. Viot, S. M. Ricci, J. Talbot, *Molec. Phys.*, **73** (1991) 773.
- [6] P. Viot, G. Tarjus, S. M. Ricci, J. Talbot, *J. Chem. Phys.*, **97** (1992) 5212.
- [7] S. M. Ricci, J. Talbot, G. Tarjus, P. Viot, *J. Chem. Phys.*, **97** (1992) 5219.
- [8] Z. Adamczyk, P. Weroński, *J. Chem. Phys.*, **105** (1996) 5562.
- [9] P. Schaaf, A. Johner, J. Talbot, *Phys. Rev. Lett.*, **66** (1991) 1603.
- [10] B. Senger, P. Schaaf, A. Johner, J.-C. Voegel, A. Schmitt, J. Talbot, *Phys. Rev., A*, **44** (1991) 6926.
- [11] B. Senger, P. Schaaf, J.-C. Voegel, A. Johner, A. Schmitt, J. Talbot, *J. Chem. Phys.*, **97** (1992) 3813.
- [12] B. Senger, J. Talbot, P. Schaaf, A. Schmitt, J.-C. Voegel, *Europhys. Lett.*, **21** (1993) 135.
- [13] R. Jullien, P. Meakin, *J. Phys., A*, **25** (1992) L189.
- [14] H. S. Choi, J. Talbot, G. Tarjus, P. Viot, *J. Chem. Phys.*, **99** (1993) 9296.
- [15] G. Tarjus, P. Viot, H. S. Choi, J. Talbot, *Phys. Rev. E*, **49** (1994) 3239.
- [16] P. Schaaf, P. Wojtaszczyk, E. K. Mann, B. Senger, J.-C. Voegel, D. Bedeaux, *J. Chem. Phys.*, **102** (1995) 5077.
- [17] Z. Adamczyk, B. Siwek, M. Zembala, P. Warszyński, *J. Colloid Interface Sci.*, **140** (1990) 123.
- [18] Z. Adamczyk, P. Weroński, *Langmuir*, **11** (1995) 4400.
- [19] Z. Adamczyk, P. Weroński, *J. Colloid Interface Sci.*, **189** (1997) 348.
- [20] M. R. Oberholzer, J. M. Stankovich, S. L. Carnie, D. Y. C. Chan, A. M. Lenhoff, *J. Colloid Interface Sci.*, **194** (1997) 138.
- [21] J. Talbot, P. Schaaf, *Phys. Rev. A*, **40** (1989) 422.
- [22] P. Meakin, R. Jullien, *Phys. Rev. A*, **46** (1992) 2029.
- [23] Z. Adamczyk, B. Siwek, M. Zembala, P. Weroński, *J. Colloid Interface Sci.*, **185** (1997) 236.
- [24] Z. Adamczyk, B. Siwek, P. Weroński, *J. Colloid Interface Sci.*, **195** (1997) 261.
- [25] Z. Adamczyk, P. Weroński, *J. Chem. Phys.*, **108** (1998) 9851.
- [26] Z. Adamczyk, P. Weroński, E. Musiał, *J. Chem. Phys.*, **116** (2002) 4665.
- [27] Z. Adamczyk, P. Weroński, E. Musiał, *J. Colloid Interface Sci.*, **248** (2002) 67.
- [28] Z. Adamczyk, *Irreversible Adsorption of Particles*, in: *Adsorption: Theory, Modeling and Analysis*, ed.: J. Toth, Marcel-Dekker, New York 2002, p. 251.
- [29] G. M. Bell, S. Levine, L. N. McCartney, *J. Colloid Interface Sci.*, **33** (1970) 335.
- [30] H. Ohshima, T. W. Healy, L. R. White, *J. Colloid Interface Sci.*, **90** (1982) 17.
- [31] J. A. Barker, D. Henderson, *J. Chem. Phys.*, **47** (1967) 4714.
- [32] W. H. Press, S. A. Teukolsky, W. T. Vetterling, B. P. Flannery, *Numerical Recipes in Fortran*, Sec. Ed. Cambridge Univ. Press 1992, p. 351.
- [33] M. Piech, J. Y. Walz, *Langmuir*, **16** (2000) 7895.
- [34] K. L. Hiebert, *Subroutine DNSQ of SLATEC Library*,
<http://www.netlib.org/slatec/>

- [35] Z. Adamczyk, B. Siwek, P. Weroński, M. Zembala, *Progr. Colloid Polym. Sci.*, **111** (1998) 41.
- [36] H. Reiss, H. L. Frisch, J. L. Lebowitz, *J. Chem. Phys.*, **31** (1959) 369.
- [37] J. L. Lebowitz, E. Helfand, E. Praestgaard, *J. Chem. Phys.*, **43** (1965) 774.
- [38] J. Talbot, X. Jin, N. H. L. Wang, *Langmuir*, **10** (1994) 1663.
- [39] P. W. Weroński, Ph. D. Thesis: *Kinetics and Topology of Irreversible Adsorption of Anisotropic Particles at Homogeneous Interfaces*, Institute of Catalysis and Surface Chemistry, Polish Academy of Science, Krakow 2000, in Polish.